

Two-dimensional spatial-phase-locked electron-beam lithography via sparse sampling

J. T. Hastings,^{a)} Feng Zhang, M. A. Finlayson, J. G. Goodberlet, and Henry I. Smith
Department of Electrical Engineering and Computer Science, Rm. 39-427, Massachusetts Institute of Technology, Cambridge, Massachusetts 02139

(Received 12 June 2000; accepted 1 August 2000)

We report a new mode of spatial-phase-locked electron-beam lithography based on alignment of each e -beam deflection field to a fiducial grid on the substrate. Before exposing the pattern in a given field, the fiducial grid is sparsely sampled with the electron beam at a subexposure dose. These samples form a two-dimensional moiré pattern that is analyzed to calculate field shift, scale, rotation, nonorthogonality, and trapezoidal distortion. Experimental verification of the approach was carried out with a scintillating fiducial grid quenched by interference lithography. Despite a poor signal-to-noise ratio, we achieved sub-beamstep field-stitching and pattern-placement accuracy.
© 2000 American Vacuum Society. [S0734-211X(00)02206-X]

I. INTRODUCTION

Spatial-phase-locked electron-beam lithography (SPLEBL) is being developed to significantly improve the pattern-placement accuracy of scanning-electron-beam lithography (SEBL) tools.¹⁻⁴ In principle, SPLEBL is capable of positioning patterns on a substrate to within 1 nm. In one-dimensional experiments, precisions of 5 nm have been achieved to date.^{2,3} Such precisions are not achieved with traditional electron-beam lithography because these systems operate open loop, i.e., the position of the electron beam on the substrate is not directly monitored. In SPLEBL, the beam position, with reference to the substrate, is monitored continuously, or semicontinuously, so that feedback can be used to eliminate sources of pattern-placement errors. Currently, SPLEBL is the only known solution for achieving sub-20 nm pattern-placement accuracy, as will soon be required by the International Technology Roadmap for Semiconductors.⁵

This article describes a new mode of SPLEBL, which employs a sparse-sampling technique and is suitable for vector-scan and raster-scan SEBL tools. Details of the sparse-sampling algorithm are presented, and its performance under various signal-to-noise ratios (SNRs) is reported. Also, we report results from the first two-dimensional (2D) SPLEBL experiment which used the sparse-sampling algorithm and a scintillating global-fiducial grid. This grid, patterned on the substrate by interference lithography, provided the necessary feedback signal for SPLEBL. Under very poor SNR conditions, field-stitching and pattern-placement precisions of less than one beam step were achieved in the 2D experiment.

II. SPARSE SAMPLING APPLIED TO SPLEBL

In the sparse-sampling mode of SPLEBL the global-fiducial grid is sampled at discrete locations within the e -beam field with a subthreshold dose, while the laser-interferometer-controlled stage, which holds the sample, is stationary. Immediately after processing the acquired data

and making field corrections, the desired pattern is written within the e -beam field. Figure 1 provides an overview of the sparse-sampling approach and shows the experimental setup appropriate for a scintillating fiducial grid.

The samples, which are taken at spacings larger than the grid period, are subthreshold and hence do not transfer in subsequent processing steps. Because the spatial frequency of the fiducial grid is higher than the spatial frequency of the sparse samples, the acquired signal will be aliased. In the spatial domain, aliased periodic signals appear as moiré patterns. Figure 2(a) shows the moiré pattern formed by sampling a 1 μm period gold grid at 512 \times 512 equally spaced points within a 528 μm field. The number of periods in the moiré is simply given by the difference between the number of sample points and the number of fiducial grid periods in a given direction, in this case exactly 16 periods in both X and Y . Higher-order aliasing produces a similar effect, i.e., 512 \times 512 samples of 1040 \times 1040 periods will also yield a 16 \times 16 period moiré pattern.

The moiré pattern provides a sensitive tool for measuring deflection-field alignment and distortion. The spatial phase of the moiré signal represents the spatial phase of the periodic sample locations with respect to the underlying fiducial grid. Thus, the deflection field can be shifted into alignment with the fiducial grid by locking the spatial phase of the moiré pattern to a specified value. Variation of the moiré phase with position in X or Y indicates a rotation, or skew, of the deflection field with respect to the grid. If this variation differs between X and Y the deflection axes are not orthogonal. The spatial frequency of the moiré pattern allows one to precisely calculate the number of periods contained in the deflection field, and thus determine the scale (magnification) of the field. A linear variation of X spatial frequency with Y , or vice-versa, indicates the presence of trapezoidal distortion.

Our SEBL system uses eight parameters to model and correct the error between desired beam position (x, y) and actual beam position (x', y') . These relationships are given by

$$x' = x_0 + S_x x + \theta_x y + T_x x y, \quad (1)$$

^{a)}Electronic mail: hastings@nano.mit.edu

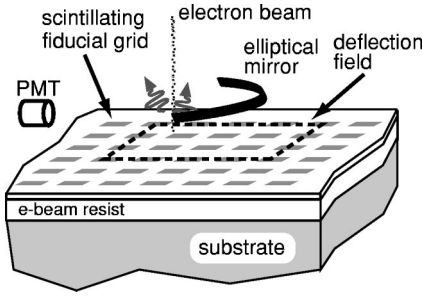


FIG. 1. Experimental setup for sparse-sampled SPLEBL. Photons produced in the electron-scintillator interaction are focused onto the photomultiplier tube (PMT) by the elliptical mirror. This depiction shows the deflection field aligned to a few fiducial grid periods. In practice, the field encompasses about 500 periods in both X and Y .

$$y' = y_0 + S_y y + \theta_y x + T_y x y,$$

where x_0 and y_0 are the field-shift errors, S_x and S_y are unitless field-scaling errors, θ_x and θ_y are the skew errors, and T_x and T_y are trapezoidal-distortion errors in units of $1/\text{length}$.

To determine the relationship between these errors and the observed moiré pattern, we begin by approximating the fiducial-grid signal as a sum of two orthogonal sinusoidal gratings. I_{grid} represents the signal level regardless of the signal type (backscattered electron, secondary electron, or photon)

$$I_{\text{grid}} \approx A_x \cos\left(\frac{2\pi}{\Lambda_G} x'\right) + A_y \cos\left(\frac{2\pi}{\Lambda_G} y'\right) + C + N, \quad (2)$$

where A is the amplitude of the modulation, C is the background level, and Λ_G is the spatial period of each grid, typically 200 nm to 1 μm . N is a simplified noise term having a Gaussian distribution with variance σ^2 . The noise term approximates the electron-arrival statistics, scintillator-photon emission statistics, photomultiplier-tube noise, other electronic noise, and stray light in the vacuum chamber. The SNR is defined as $(A_x^2 + A_y^2)/\sigma^2$. Neglecting the noise term and substituting Eq. (1) into Eq. (2), we obtain a function describing the appearance of the fiducial grid within a misaligned or distorted field.

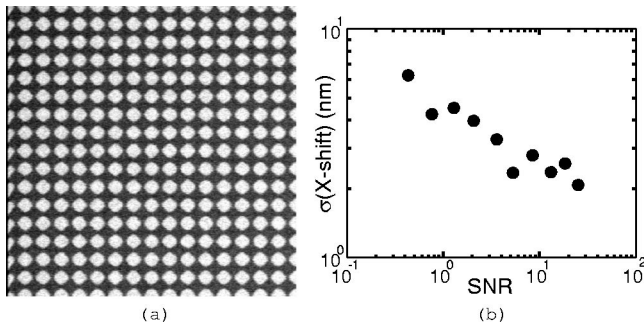


FIG. 2. (a) Moiré pattern obtained from 512 \times 512 backscattered electron samples of a 528 μm field with a 1 μm period gold grid. (b) Standard deviation of x shift error estimates vs SNR using the grid shown in (a).

If we take the Fourier transform of Eq. (2) with respect to x at arbitrary y , we find that the spatial phase and frequency of the fundamental Fourier component are given by

$$\phi_x = \frac{2\pi}{\Lambda_G} (x_0 + \theta_x y), \quad (3)$$

$$f_x = \frac{1}{\Lambda_G} (S_x + T_x y). \quad (4)$$

We see that both phase and frequency are linear functions of y , with slopes $(2\pi/\Lambda_G)\theta_x$ and T_x/Λ_G and intercepts $(2\pi/\Lambda_G)x_0$ and S_x/Λ_G , respectively. When undersampling the fiducial grid the phase of the moiré pattern along an axis ϕ_{xm} remains identical to that of the fiducial grid, but aliasing must be taken into account for the moiré frequency f_{xm} . Therefore,

$$\phi_{xm} = \frac{2\pi}{\Lambda_G} (x_0 + \theta_x y), \quad (5)$$

$$f_{xm} = \left| \frac{1}{\Lambda_G} (S_x + T_x y) - \frac{1}{\Lambda_S} \right|, \quad (6)$$

where Λ_S is the spatial period of the sparse samples.

After acquiring the moiré pattern via an array of discrete samples, we estimate its phase and frequency with respect to x at several y positions. This is accomplished using one-dimensional discrete Fourier transforms (DFTs) and a simple peak-search routine for each row of data. Because the moiré spatial frequency is approximately known before beginning the analysis, one need only compute the amplitude at a few frequencies to estimate the peak position with high precision. This proves more computationally efficient than a large zero-padded fast-Fourier transform. After performing linear least-squares fits of the phase and frequency versus y , the field corrections are given by

$$x_0 = \frac{\Lambda_G}{2\pi} \phi_{xm} \Big|_{(y=0)},$$

$$\theta_x = \frac{\Lambda_G}{2\pi} \frac{d\phi_{xm}}{dy}, \quad (7)$$

$$S_x = \Lambda_G \left(f_{xm} \Big|_{y=0} + \frac{1}{\Lambda_S} \right),$$

$$T_x = \Lambda_G \frac{df_{xm}}{dy}.$$

The corresponding field corrections for Y can be found in the same manner.

Variation of the signal-detection efficiency across the deflection field leads to nonuniformities in the moiré pattern. These variations add low-spatial-frequency spectral components that introduce bias in the error estimates described above. To reduce this effect we least-squares fit a 2D polynomial to the signal level across the field. When each field is sampled the signal is divided by this detection efficiency function to reduce the bias errors.

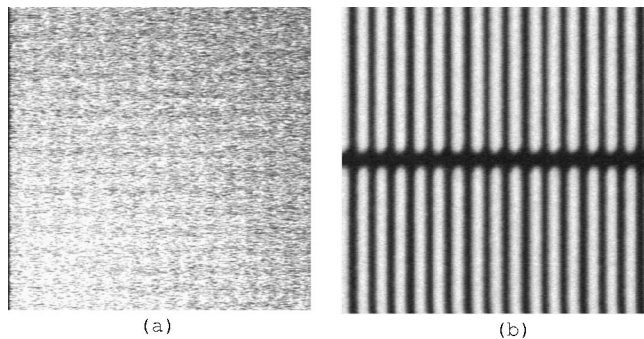


FIG. 3. Results from field stitching experiment: (a) Moiré pattern used for locking: 512×512 samples of $280 \mu\text{m}$ field with a 530 nm period scintillating grid; (b) backscattered-electron image of stitched gold gratings at a field boundary. The gap was intentionally included to make the location of the boundary clear.

If the signal acquired from the fiducial grid has a low SNR, a single row or column of sample points may not reach the SNR threshold level for accurate spectral peak identification. In this case several rows may be averaged together to increase the SNR before performing the DFTs. This technique is also important if the fiducial grid deviates from a simple sum of sinusoids, e.g., an array of metallic dots, where certain rows or columns of samples may have no signal at all. Finally, the averaged data are multiplied by a Hann (squared cosine) window before Fourier transforming to further reduce interference from any residual low frequency signals.

The performance of this algorithm was verified in our SEBL system, VS2A, by repeatedly locking to a $1 \mu\text{m}$ period gold fiducial grid at one position. Adjusting the beam current allows the variance of the parameter estimates to be measured at several SNRs. Estimation theory indicates that beyond a certain threshold level the variance σ^2 of sinusoid phase and frequency estimates decreases as SNR^{-1} . The field-correction parameters should change little between locking cycles, but any system instability on this time scale (a few seconds) will be observed as a lower limit on the variance of parameter estimate values. The variance, σ^2 of all field correction parameters, was found to decrease as $\text{SNR}^{-1 \pm 0.06}$ except for field shift. Figure 2(b) shows the standard deviation of the X -shift estimate versus SNR. The shift variance does not decrease uniformly because of fluctuations introduced by interferometer quantization (5 nm), field correction unit quantization ($4 \text{ nm} = 1/8$ beam step), and system drift on the time scale of the corrections.

III. FIELD-STITCHING EXPERIMENTS

Field-stitching experiments to verify the approach described above were conducted on our SEBL system. The system operates at 50 keV , uses 14-bit resolution deflection fields, and has a $\lambda/128$ laser-interferometer-controlled stage. A scintillating fiducial grid was used for these experiments.⁶ The grid consists of a poly(methylmethacrylate)-based resist with additional components that scintillate when struck by

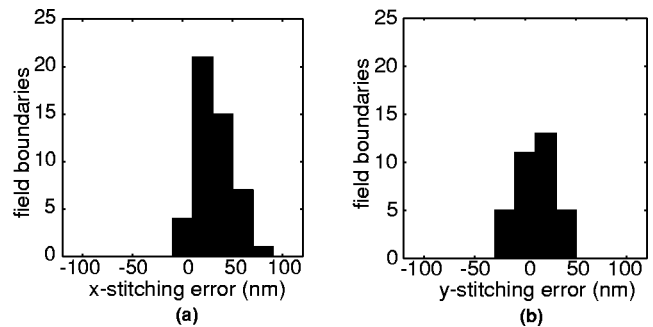


FIG. 4. Stitching error histograms for both X (a) and Y (b) using the 530 nm period scintillating grid. $1 e\text{-beam-step} = 17 \text{ nm}$, $\sigma_x = 17 \text{ nm}$, $\sigma_y = 18 \text{ nm}$.

electrons. The scintillation can be quenched by exposure to ultraviolet light without exposing the resist. The scintillating fiducial grid requires no sacrifice of substrate area and is quenched instead of physically patterned, so the sample remains completely planar.

Silicon wafers were coated with 400 nm of the scintillating resist, and orthogonal gratings were quenched using 351 nm light from an Ar ion laser in our interference lithography system.⁷ Interference lithography (IL) relies on the standing wave generated when two plane, or spherical, waves interfere at an angle. The use of IL guarantees the spatial coherence of the grid, and the period is precisely determined by the wavelength and angle of intersection.

As the electron beam samples the fiducial grid, the light from the electron–scintillator interaction is collected with an elliptical mirror and focused onto a photomultiplier tube (PMT), as indicated in Fig. 1. The PMT signal is amplified and routed to an image acquisition board in the host computer. The image processing of the captured moiré pattern is carried out using an Alacron AL860MP array processor board.

Figure 3(a) shows a 16×16 moiré pattern obtained from a 530 nm period scintillating fiducial grid, sampled over a $280 \mu\text{m}$ field. The SNR was ≈ 0.09 for the scintillating grid, as opposed to ≈ 25 for the $1 \mu\text{m}$ gold grid [Fig. 2(a)] when sampled at the same dwell time and beam current. The SEBL tool's constrained vacuum chamber makes light collection difficult, thus the low SNR observed for the scintillating grid.

In actual pattern-placement experiments, the SNR of the scintillating grid was too low to permit accurate rotation, scaling, and trapezoidal correction for each field. Trapezoidal distortion was corrected using a traditional field-calibration routine, and rotation and scale were fixed to their initial values after applying the sparse-sampling routine to one deflection field. Shift correction was enabled for all fields.

To test stitching and pattern placement, we exposed an array of $280 \mu\text{m}$ $e\text{-beam}$ fields with 400 nm period gratings at the field boundaries. An intentional gap was left between the gratings so that the field boundary could be easily identified. These gratings were transferred to the substrate by gold evaporation and liftoff, and subsequently imaged at high magnification in the same SEBL system. A backscat-

tered electron image of the stitched gratings is shown in Fig. 3(b).

The stitching error between fields was measured using a technique developed by Ferrera *et al.*² which determines the spatial-phase difference between the two gratings. The phase of each grating is measured by taking the Fourier transform of its image and finding the phase at the fundamental peak. The stitching error Δ_{st} is given by

$$\Delta_{st} = \Lambda_{\text{grat}} \frac{\phi_2 - \phi_1}{2\pi}, \quad (8)$$

where ϕ_2 and ϕ_1 are the spatial phases on each side of the boundary, and Λ_{grat} is the spatial period of the patterned grating. Because of the high magnification and favorable SNR of these images, the stitching error can be measured to $\sigma = 3$ nm. Figure 4 shows histograms of the measured stitching errors in both X and Y . The standard deviation of the stitching errors was 17 and 18 nm for X and Y , respectively, while the mean errors were 31 and 10 nm for X and Y . One beam step in the 280 μm deflection field is equal to 17 nm. The large mean values are a direct result of not correcting rotation for each field, and should be greatly reduced with an improvement to the 0.09 SNR of these experiments.

The patterns were written aligned to the fiducial grid, so there is no cumulative error or placement drift across the substrate. As a result, stitching errors translate directly into pattern-placement error with respect to the grid. Given a placement error of σ_{pp} , stitching error is given by $\sigma_{st} = \sqrt{2} \sigma_{pp}$. We find that the pattern placement for the experiment above is $\sigma_x = 12$ nm and $\sigma_y = 13$ nm.

IV. CONCLUSION

Spatial-phase-locked e -beam lithography provides a route to pattern-placement accuracy beyond that of traditional e -beam tools. An algorithm has been developed which al-

lows alignment of the deflection field to the fiducial grid using a moiré pattern obtained by sub-exposure-dose sparse sampling. This mode of SPLEBL provides 2D sub-beam-step pattern placement, even with an extremely poor SNR. Improvements to the scintillator and the light collection system will increase SNR and pattern-placement accuracy. Further improvements in pattern placement will be obtained with a finer period fiducial grid.

In the future, sparse sampling will be extended to raster-scan systems using a quasicontinuous feedback mode. The sparse samples will be obtained whenever the beam passes over a desired sample point. In this way correction parameters can be updated more frequently. Ultimately, 1 nm pattern placement could be achieved by continuously sampling the grid throughout the pattern exposure.

ACKNOWLEDGMENTS

The authors gratefully acknowledge J. Carter, J. Daley, and M. Mondol for their valuable technical assistance. This research was sponsored by the Defense Advanced Research Projects Agency and the Army Research Office under Contract No. DAAD19-99-1-0280. The views expressed here are not endorsed by the sponsors.

¹H. I. Smith, S. D. Hector, M. L. Schattenburg, and E. H. Anderson, *J. Vac. Sci. Technol. B* **9**, 2992 (1991).

²J. Ferrera, V. Wong, S. Rishton, V. Boegli, E. H. Anderson, D. P. Kern, and H. I. Smith, *J. Vac. Sci. Technol. B* **11**, 2342 (1993).

³J. G. Goodberlet, J. Ferrera, and H. I. Smith, *J. Vac. Sci. Technol. B* **15**, 2293 (1997).

⁴J. T. Hastings, F. Zhang, J. G. Goodberlet, and H. I. Smith, *Microelectron. Eng.* **53**, 361 (2000).

⁵*International Technology Roadmap for Semiconductors*, 1999 ed. (Semiconductor Industry Association, 1999), <http://www.itrs.net/ntsr/publntsr.nsf>

⁶J. G. Goodberlet, J. Carter, and H. I. Smith, *J. Vac. Sci. Technol. B* **16**, 3672 (1998).

⁷J. Ferrera, M. L. Schattenburg, and H. I. Smith, *J. Vac. Sci. Technol. B* **14**, 4009 (1996).